FEBS Letters

FEBS PRESS science publishing by scientists

REVIEW

Novel insights into autophagosome biogenesis revealed by cryo-electron tomography

Eeva-Liisa Eskelinen

Institute of Biomedicine, University of Turku, Finland

Correspondence
E.-L. Eskelinen, Institute of Biomedicine, University of Turku, Kiinamyllynkatu 10, Medisiina C341, 20520 Turku, Finland
Tel: +358505115631
E-mail: eeva-liisa.eskelinen@utu.fi

(Received 10 July 2023, revised 11 August 2023, accepted 14 August 2023, available online 3 September 2023)

doi:10.1002/1873-3468.14726

Edited by Michael Thumm

Autophagosome biogenesis, from the appearance of the phagophore to elongation and closure into an autophagosome, is one of the long-lasting open questions in the autophagy field. Recent studies utilising cryo-electron tomography and detailed analysis of the image data have revealed new information on the membrane dynamics of these events, including the shape and dimensions of omegasomes, phagophores and autophagosomes, and their relationships with the organelles around them. One of the important predictions from the new results is that 60–80% of the autophagosome membrane area is delivered by direct lipid transfer or lipid synthesis. Cryo-electron tomography can be expected to provide new directions for autophagy research in the near future.

Keywords: autophagosome; cryo-electron tomography; electron microscopy; focused ion beam milling; omegasome; phagophore

Autophagosome biogenesis involves membrane dynamics that is not fully understood. Autophagosomes are known to be formed by phagophores, flat membrane cisterns that elongate and wrap around the cytoplasmic cargo. The closure of the rim of the phagophore completes the formation of a double-membrane limited autophagosome. Electron microscopy has revealed that phagophores emerge close to the endoplasmic reticulum (ER) and can have membrane contact sites or continuities with the ER [1,2]. Live-cell imaging was used to show that autophagosome biogenesis occurs in ER subdomains called omegasomes, omega-shaped structures positive for the protein DFCP1 [3]. In conventional electron microscopy samples, omegasomes were described to consist of tubular/vesicular or cisternal connections between the ER and the phagophore [4,5].

The autophagy protein ATG9 is essential for autophagosome biogenesis; ATG9-positive vesicles form seeds for phagophore initiation [6,7]. The elongation of the phagophore membrane is mediated by lipid transfer from the ER by ATG2 (Atg2 in yeast) [8,9], which is a rod-shaped lipid transfer protein [8,10–12]. In yeast, also Vps13 functions to assist lipid transfer to growing phagophores [13]. The lipid transfer from the ER is facilitated by two ER-associated scramblases, VMP1 and TMEM41B [14]. In yeast, Atg9 is needed for Atg2-dependent contact sites between the ER and the phagophore [15]. The association of the mammalian ATG9A with ATG2 (ATG2A and ATG2B) is crucial for phagophore biogenesis [16]. ATG9A functions as a scramblase that mediates lipid translocation from the cytoplasmic to luminal leaflet of the lipid bilayer [17,18]. ATG2 proteins are thought to transport lipids from the ER to the cytoplasmic leaflet of the growing phagophore membrane. ATG9A could then distribute the lipids to the luminal leaflet in order to facilitate phagophore elongation (reviewed in [19]).

Autophagosome biogenesis is a relatively rapid process. Therefore, ultrastructural details of the membrane dynamics are difficult to capture by electron microscopy using conventional sample preparation involving chemical fixation. Chemically fixed samples also need dehydration that causes further alterations in the morphology of membrane-bound organelles. Recent

Abbreviations
ER, endoplasmic reticulum; ET, electron tomography; SCV, *Salmonella*-containing vacuole.

studies performed using the advanced sample preparation technique called cryo-electron tomography (cryo-ET) [20–22] (Fig. 1) have revealed previously unknown features of phagophore morphology and the connections of phagophores with the ER. This technique utilises cryofixation, which relies on vitrification of the cells into amorphous ice within milliseconds [23,24]. Cryofixation has several advantages compared to chemical fixation. Firstly, it is able to capture very short-lived events. Secondly, it immobilizes all macromolecules simultaneously, unlike chemical fixation that immobilizes lipids and carbohydrates incompletely. Thirdly, cryofixation is free of so-called fixation artefacts and alterations caused by dehydration, which mainly affect lipid-rich structures such as biological membranes [24]. After cryofixation, the samples are imaged without further sample preparation, excluding possible thinning with focused ion beam milling in order to make the sample thin enough for the electron beam to pass through (Fig. 1). Three-dimensional information is collected using cryo-ET by tilting the sample in the cryo-electron microscope in order to acquire images in different angles [20,25]. The tilt-series images are then combined to create three-dimensional reconstruction images of the sample. The correlation of fluorescence and electron microscopy images can be used to enable localisation and identification of the rear and short-lived nascent phagophores in cells [21]. This article summarises recent findings on autophagosome biogenesis and morphology made using cryo-ET.

Novel features of phagophore morphology in starvation-induced autophagy

Bieber *et al.* [26] analysed phagophore morphology in the yeast *Saccharomyces cerevisiae*. Autophagy was induced by nitrogen starvation, and phagophores were identified using overexpression of fluorescent-protein tagged Atg8, a marker for both phagophores and autophagosomes. Alternatively, identification was assisted by overexpressing GFP-tagged selective autophagy substrate Ede1, either alone on together with mCherry-tagged Atg8. The earliest phagophores were observed as slightly bent flat membrane cisterns (Fig. 2A,B). More elongated phagophores and closed autophagosomes were also imaged and analysed. By comparing the density of ribosomes inside and outside the elongating phagophores, Bieber *et al.* concluded that under nitrogen starvation, phagophores engulf cytosol nonselectively, without a detectable cargo that could serve as a template.

Further, Bieber *et al.* [26] quantitatively analysed the morphology of phagophores and autophagosomes. Autophagosomes were observed to be almost perfectly spherical while phagophores were elongated, assuming a more ellipsoidal shape. The distance between the inner and outer membrane was measured and quantified. Interestingly, the analysis revealed that the intermembrane distance of phagophores decreased during autophagosome biogenesis. Further, the intermembrane distance of autophagic membranes was observed to be significantly smaller than in mitochondria, the nuclear membrane and ER sheets. In closed autophagosomes, the distance between the two limiting membranes was uniform 9–11 nm. The ratio of total membrane area to intermembrane lumen volume of autophagosomes was calculated to be $0.53 \pm 0.10\ nm^{-1}$. Two processes have been suggested to support phagophore elongation, vesicle fusion and direct lipid transfer, of which only vesicle fusion can add volume to the intermembrane space. Taking into account the size of the vesicles that are thought to deliver membrane to phagophores, Atg9 vesicles and

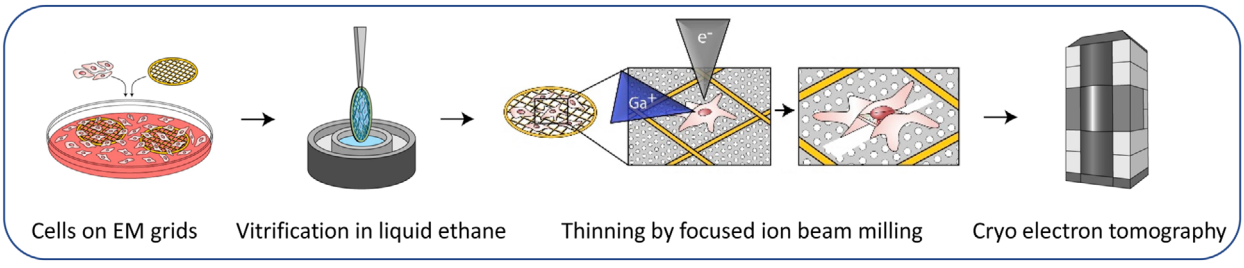

Fig. 1. Workflow for cryo-ET. Cells are grown on an electron microscopy grid or attached to the grid if grown in suspension. The cells are vitrified using either plunge freezing in liquid ethane or high-pressure freezing (not shown). Thin areas in the cell periphery of adherent cells can be imaged with ET without thinning. Thicker regions of the cells need to be thinned using focused ion beam milling, after which a thin lamella of cytoplasm is left. Cryo fluorescence microscopy after vitrification and thinning can be used to locate structures of interest in correlative light-electron microscopy workflow (not shown). The figure is reproduced, with permission from the corresponding author, from fig. 3A in Weber *et al.* [44], published under CC BY license (http://creativecommons.org/licenses/by/4.0/).

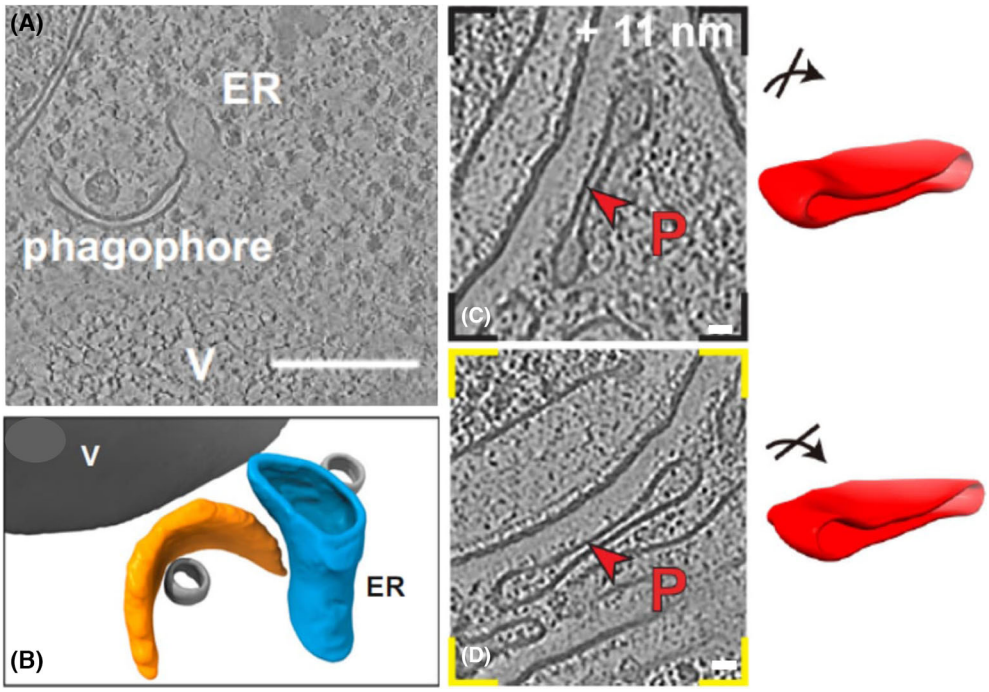

Fig. 2. Cryo-ET images of early phagophores in *Saccharomyces* (A, B) and HeLa cells (C, D). (A, B) A tomographic slice showing a phagophore in yeast (A). A three-dimensional model of the region shown in panel A (B, note that the image is upside down compared to panel A). The phagophore is in orange. V, vacuole. Scale bar, 200 nm. Panels A and B are reproduced, with modifications and with permission from the authors, from fig. 1E,I in Bieber *et al.* [26], published under CC BY-NC-ND license (https://creativecommons.org/licenses/by-nc-nd/4.0/). (C, D) The red arrowheads indicate early phagophores (P) in HeLa cells. The three-dimensional models of the phagophores in C and D are shown on the right. Scale bars, 20 nm. Panels C and D are reproduced, with permission from the corresponding author, from fig. 1F in Li *et al.* [27], published under CC BY license (https://creativecommons.org/licenses/by/4.0/).

COPII vesicles, as well as the observed intermembrane space of autophagosomes, Bieber *et al.* concluded that vesicle fusion would not contribute enough membrane to build the whole autophagosome. The data thus suggested that 60–80% of the membrane area is delivered by direct lipid transfer or lipid synthesis.

Bieber *et al.* [26] also reported novel features on the phagophore membrane morphology. The phagophore rims were observed to be dilated (Fig. 2A). Detailed analysis using artificial, nondilated rims showed that dilation decreases the bending energy at the rim, which is likely to help in stabilising the open phagophore. The dilated rims of phagophores were also observed in cryo-ET samples of HeLa cells during selective autophagy of intracellular bacteria [27]. In HeLa cells, the rim dilation was even more pronounced than in yeast (Fig. 2C,D). Phagophore rim dilation is also visible in cryo-ET images of HeLa cells undergoing selective autophagy of protein condensates in Ref. [28], although this study did not analyse the rim morphology.

Cryo-ET revealed details on phagophore membrane contact sites

Bieber *et al.* [26] analysed the contacts of the phagophores with other organelles in detail. Contacts were defined as a minimum distance of 100 nm or less between the two membranes. Membrane deformations in the phagophore were assumed to indicate specific interaction between the phagophore and the other organelle because deformations imply that additional forces have caused them. In agreement with previous knowledge, cryo-ET revealed contacts between phagophores and the vacuole. Novel aspects of the vacuole-phagophore membrane contact sites were reported. Firstly, contacts were observed exclusively between the back and side of the phagophore, while the rim made no contact with the vacuole. In half of the contacts, the phagophore membrane showed deformations, including a peak-like extension towards the vacuole, or close contact with the vacuole over an extended area. These findings support the notion that phagophores are physically tethered to the vacuole.

The phagophore rims were frequently observed in contact with the ER or nuclear membrane in yeast cells [26]. No strong deformations were observed in phagophore rims close to the ER (Fig. 3A) while contacts with the nuclear membrane showed deformation of the rim towards the nuclear membrane (Fig. 3B). The frequent contacts between the phagophore rim and ER are in agreement with the proposed lipid transfer from the ER to the phagophore [9,12]. In part of the cryo tomograms, the phagophore rim and the ER or nuclear membrane were connected by stick-like structures that were 17 ± 3 nm long (Fig. 3A,B,A′,B′) [26], which is close to the length of yeast Atg2 [29]. The stick-shaped structures were, however, too heterogenous and rare to allow more detailed analysis by subtomogram averaging. Notably, similar stick-like 16–21 nm long connections between the phagophore rim and ER were reported by Carter *et al.* [28] by cryo-ET of selective autophagy of protein condensates in HeLa cells. Further, Li *et al.* [27] frequently observed membrane contact sites between the phagophore rim and ER by cryo-ET of selective autophagy of intracellular bacteria in HeLa cells. The contact sites were occupied by stick-like densities that connected the two organelles (Fig. 3C). The average length of the densities was 19.0 ± 3.9 nm, which is close to the length of the mammalian ATG2 protein [30]. In addition, Li *et al.* [27] also observed other types of densities between the dilated phagophore rims and ER, suggesting that several types of membrane contact sites may exist between the phagophore and ER.

Lipid droplets have also been suggested to deliver additional lipids for phagophore elongation [31]. In cryo-ET images of yeast, Bieber *et al.* [26] observed lipid droplets next to phagophores, but they did not show a preferred interaction site in the phagophores. Occasional deformations were observed in the phagophore membrane in these contact sites, which suggests that the contacts may be rare but functional.

Novel features of phagophores and omegasomes in selective autophagy

Li *et al.* [27] used cryo-ET to analyse the three-dimensional morphology of phagophores and autophagosomes in

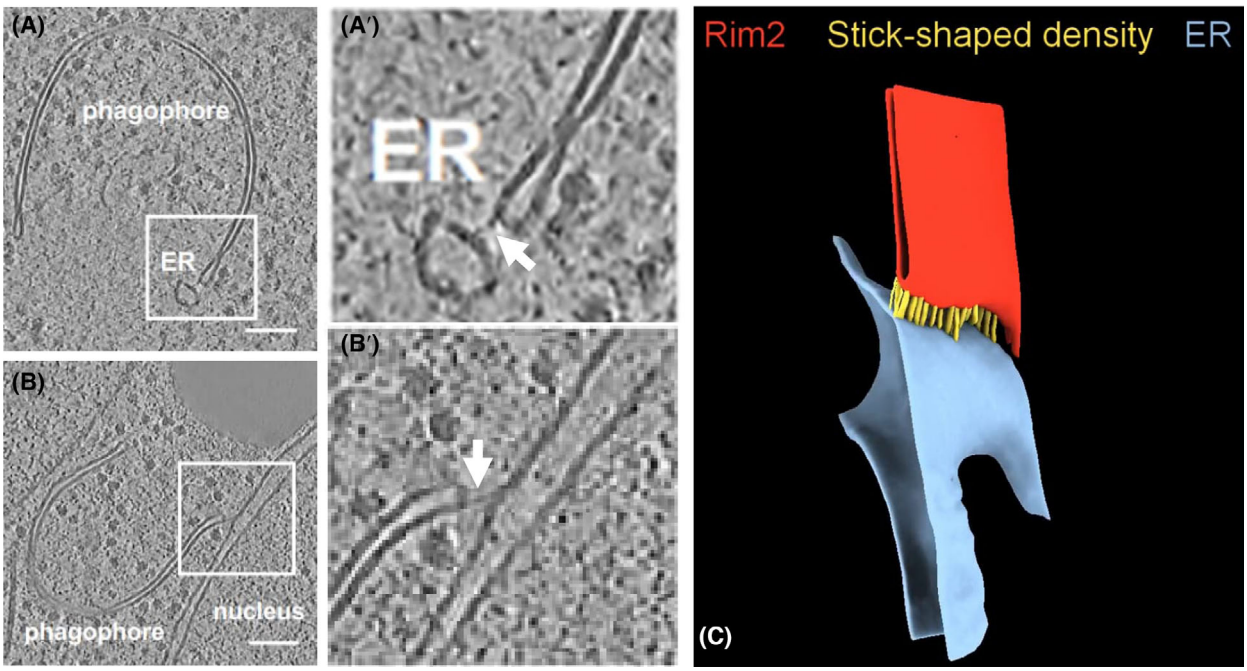

Fig. 3. Cryo-ET images and a model of membrane contact sites between phagophore rims and the ER in *Saccharomyces* (A, A′, B, B′) and HeLa cells (C). (A, B) Tomographic slices showing stick-like connections between the phagophore rim and ER (A) or the phagophore rim and the nuclear membrane (B) in yeast (boxes). The boxed areas are enlarged in panels A′ and B′, where the stick-like structures are indicated by arrows. Bars in A and B, 100 nm. Panels A, A′, B and B′ are reproduced, with modifications and with permission from the authors, from fig. 4E(i),F(i) in Bieber *et al.* [26], published under CC BY-NC-ND license (https://creativecommons.org/licenses/by-nc-nd/4.0/). (C) A three-dimensional model of a membrane contact site between the phagophore rim (red) and ER (blue) in a HeLa cell. The stick-like structures connecting the phagophore rim and ER are in yellow. Panel C is a screenshot from movie S4 in Li *et al.* [27], published under CC BY license (https://creativecommons.org/licenses/by/4.0/). Reproduction with permission from the corresponding author.

HeLa cells during selective autophagy of intracellular *Salmonella*. *Salmonella* bacteria enter the host cells by phagocytosis, and then reside inside *Salmonella*-containing vacuoles (SCVs). Rupture of the SCV limiting membrane exposes the bacteria to the cytosol, which initiates a selective autophagy process [32]. Li *et al*. used expression of GFP-tagged LC3B to identify phagophores in correlative light-electron microscopy workflow. The earliest observed LC3B-positive phagophores were disc-shaped, unlike the bent phagophores observed in yeast cells by Bieber *et al*. [26] (Fig. 2A–D). In addition, Li *et al*. [27] observed granular electron densities inside the dilated rims of the phagophores, suggesting that proteins may exist in this space. Multiple phagophores were observed around the same bacterium or ruptured SCV, which suggests that the autophagosome may be formed by fusion of several phagophores initiated simultaneously. In some cases, phagophores were seen on top of existing phagophores. The average distance between the cargo surface and the phagophore was 39.7 ± 10.7 nm for SCV and 37.0 ± 8.5 nm for the bacterial outer membrane, indicating a close connection between the phagophore and cargo.

Li *et al*. [27] further used the omegasome marker DFCP1 with mCherry tag in order to study the morphology of these elusive structures in cryo-ET samples. Special types of cisternal elements were observed to correspond the DFCP1 fluorescence in cryo-ET samples; they were called omegasome-like structures. The omegasome-like cisterns showed an ER-like appearance, but unlike ER, they had an electron-lucent intermembrane lumen, which was also typical for phagophores. Unlike phagophores, the omegasome-like structures showed no internal granular densities inside the rims. The omegasome-like structures were, however, tightly associated with the ER, but no direct membrane continuity with ER was observed. Instead, varying types of electron densities were found to connect the omegasome-like cisterns with the ER, suggesting some type(s) of membrane contact sites. The intermembrane distance of the DFCP1-positive structures was 23.1 ± 4.7 nm, which is larger than that in elongated phagophores having the intermembrane distance of 12.6 ± 1.2 nm. The omegasome-like cisterns were located 52.7 ± 13.5 nm from the ruptured SCV or bacterial outer membrane, which is further away than the phagophores (37.0–39.7 nm, see above). The limited tomogram volume in cryo-ET did not allow the visualisation of the whole omegasome volumes [27]. Therefore, it was not possible to study whether the omegasome-like structures formed an omega-shaped arrangement described by live-cell imaging by Axe *et al*. [3]. Notably, the cisternal morphology of the omegasome-like structures described by Li *et al*. [27] using cryo-ET of selective autophagy differs from the vesicular-tubular ultrastructure described by Uemura *et al*. [4] for DFCP1-positive omegasomes in starvation-induced autophagy in chemically fixed mouse embryonic fibroblasts. However, Gudmundsson *et al*. [5] described cistern-like morphology for DFCP1-positive omegasomes in chemically fixed HEK293 cells in starvation-induced autophagy. Thus, it is possible that the morphology of omegasomes may differ between different cell types.

Vault complexes and hexagonal nets undergo selective autophagy

Vaults are 70 × 30 nm ellipsoidal ribonucleoprotein complexes. They localise in the cytoplasm and nucleus and house noncoding vault RNAs that are important for autophagy regulation [33]. Vault RNAs directly bind the autophagy receptor protein p62/SQSTM1, thus interfering its oligomerization, which in turn is important for the function of p62 in autophagy. TRIM5α forms cytoplasmic bodies that play a role in restricting retroviral infections, and it has been shown to act as a selective autophagy receptor for viral capsid protein [34]. Carter *et al*. [28] used cryo-ET of HeLa cells overexpressing YFP-tagged TRIM5α to study selective autophagy of TRIM5α and the localisation of vaults during this process. Because vaults have a unique morphology, they were readily identifiable in the cryo-ET images [28]. Notably, while no vaults were seen in control cells not expressing YFP-tagged TRIM5α, they were frequently observed in the cells overexpressing YFP-tagged TRIM5α. Vaults were observed in the cytoplasm, as well as inside protein condensates (called sequestosomes), and inside phagophores, autophagosomes and autolysosomes. Carter *et al*. [28] concluded that vaults are recruited before the formation of visible sequestosomes, which is in agreement with their interaction with p62. Interestingly, the sequestosome condensates that correlated with YFP-tagged TRIM5α fluorescence, showed a hexagonal net structure with a lattice spacing of 29 nm from the centre of one hexagon to the centre of the next one. This lattice spacing is similar to that formed by purified TRIM5α hexamers [35]. The results showed that TRIM5α forms hexagonal lattices in the cytoplasmic sequestosomes, that the sequestosomes also contain vaults, and that they can undergo selective autophagy. Future studies are needed to decipher the exact function of the hexagonal TRIM5α nets in selective autophagy.

Conclusions and perspectives

Because most biological samples are too thick for direct imaging in transmission electron microscopy, focused ion beam milling is used to prepare lamellae of 300 nm thickness or less to enable cryo-ET. This process is time-consuming and prone to contamination, and the number of lamellae that can be prepared from one grid is limited [36]. Recent technology advances in the cryo correlative light-electron microscopy equipment [37] and preparation of the thin lamellae, including automated and streamlined cryo focused ion beam milling [38,39] and plasma-focused ion beam milling [36] can be expected to facilitate faster preparation of lamellae with less contamination. These advances will increase the availability of cryo-ET and allow it to be used for addressing questions that need high throughput. Further, cryo-ET can also be applied to study samples from multicellular organisms, using high-pressure freezing to vitrify the specimen and a technology called lift-out to extract lamellae from targeted regions [40].

Cryo-ET has revealed novel morphologic features of phagophores that were not possible to reliable acquire using chemically fixed samples, including the unique intermembrane spacing of phagophores and autophagosome limiting membranes, as well as the dilated rims of the phagophores. These novel findings enabled important predictions on the delivery of lipids for phagophore elongation. Stick-like connections between the phagophores and ER have also been reported using chemically fixed samples [5,41], but they have now been reliably confirmed and further defined using cryo-ET. Cryo-ET, subtomogram averaging and molecular modelling were recently used to solve the three-dimensional molecular organization of the ER-mitochondria encounter structure forming connections between the ER and mitochondria in yeast cells [42]. Similar approaches can be expected to solve the molecular identity of the phagophore-ER contact sites in the near future.

Due to the recent technology advances, cryo-ET can be expected to facilitate addressing several of the unsolved questions in phagophore biogenesis and autophagy [43]. These questions include the morphology of the earliest phagophore precursors and the relationship of ATG9 and COPII vesicles to phagophore initiation and elongation; the functional relationship of ATG9, ATG2 and their binding partners in the phagophore-ER contact sites; the role and molecular organisation of other organelles and membrane contact sites in the initiation and elongation of phagophores; the mechanism and molecular machinery of autophagosome closure; and the role and molecular organisation of autophagy receptors in antiviral autophagy and other types of selective autophagy.

References

1 Hayashi-Nishino M, Fujita N, Noda T, Yamaguchi A, Yoshimori T and Yamamoto A (2009) A subdomain of the endoplasmic reticulum forms a cradle for autophagosome formation. *Nat Cell Biol* **11**, 1433–1437.

2 Yla-Anttila P, Vihinen H, Jokitalo E and Eskelinen EL (2009) 3D tomography reveals connections between the phagophore and endoplasmic reticulum. *Autophagy* **5**, 1180–1185.

3 Axe EL, Walker SA, Manifava M, Chandra P, Roderick HL, Habermann A, Griffiths G and Ktistakis NT (2008) Autophagosome formation from membrane compartments enriched in phosphatidylinositol 3-phosphate and dynamically connected to the endoplasmic reticulum. *J Cell Biol* **182**, 685–701.

4 Uemura T, Yamamoto M, Kametaka A, Sou YS, Yabashi A, Yamada A, Annoh H, Kametaka S, Komatsu M and Waguri S (2014) A cluster of thin tubular structures mediates transformation of the endoplasmic reticulum to autophagic isolation membrane. *Mol Cell Biol* **34**, 1695–1706.

5 Gudmundsson SR, Kallio KA, Vihinen H, Jokitalo E, Ktistakis N and Eskelinen EL (2022) Morphology of phagophore precursors by correlative light-electron microscopy. *Cell* **11**, 3080.

6 Mari M, Griffith J, Rieter E, Krishnappa L, Klionsky DJ and Reggiori F (2010) An Atg9-containing compartment that functions in the early steps of autophagosome biogenesis. *J Cell Biol* **190**, 1005–1022.

7 Sawa-Makarska J, Baumann V, Coudevylle N, von Bulow S, Nogellova V, Abert C, Schuschnig M, Graef M, Hummer G and Martens S (2020) Reconstitution of autophagosome nucleation defines Atg9 vesicles as seeds for membrane formation. *Science* **369**, eaaz7714.

8 Maeda S, Otomo C and Otomo T (2019) The autophagic membrane tether ATG2A transfers lipids between membranes. *Elife* **8**, e45777.

9 Kotani T, Kirisako H, Koizumi M, Ohsumi Y and Nakatogawa H (2018) The Atg2-Atg18 complex tethers pre-autophagosomal membranes to the endoplasmic reticulum for autophagosome formation. *Proc Natl Acad Sci USA* **115**, 10363–10368.

10 Osawa T, Ishii Y and Noda NN (2020) Human ATG2B possesses a lipid transfer activity which is accelerated by negatively charged lipids and WIPI4. *Genes Cells* **25**, 65–70.

11 Valverde DP, Yu S, Boggavarapu V, Kumar N, Lees JA, Walz T, Reinisch KM and Melia TJ (2019) ATG2 transports lipids to promote autophagosome biogenesis. *J Cell Biol* **218**, 1787–1798.

12 Osawa T, Kotani T, Kawaoka T, Hirata E, Suzuki K, Nakatogawa H, Ohsumi Y and Noda NN (2019) Atg2 mediates direct lipid transfer between membranes for autophagosome formation. *Nat Struct Mol Biol* **26**, 281–288.
13 Dabrowski R, Tulli S and Graef M (2023) Parallel phospholipid transfer by Vps13 and Atg2 determines autophagosome biogenesis dynamics. *J Cell Biol* **222**, e202211039.
14 Ghanbarpour A, Valverde DP, Melia TJ and Reinisch KM (2021) A model for a partnership of lipid transfer proteins and scramblases in membrane expansion and organelle biogenesis. *Proc Natl Acad Sci USA* **118**, e2101562118.
15 Gomez-Sanchez R, Rose J, Guimaraes R, Mari M, Papinski D, Rieter E, Geerts WJ, Hardenberg R, Kraft C, Ungermann C *et al.* (2018) Atg9 establishes Atg2-dependent contact sites between the endoplasmic reticulum and phagophores. *J Cell Biol* **217**, 2743–2763.
16 Tang Z, Takahashi Y, He H, Hattori T, Chen C, Liang X, Chen H, Young MM and Wang HG (2019) TOM40 targets Atg2 to mitochondria-associated ER membranes for phagophore expansion. *Cell Rep* **28**, 1744–1757.e5.
17 Maeda S, Yamamoto H, Kinch LN, Garza CM, Takahashi S, Otomo C, Grishin NV, Forli S, Mizushima N and Otomo T (2020) Structure, lipid scrambling activity and role in autophagosome formation of ATG9A. *Nat Struct Mol Biol* **27**, 1194–1201.
18 Matoba K, Kotani T, Tsutsumi A, Tsuji T, Mori T, Noshiro D, Sugita Y, Nomura N, Iwata S, Ohsumi Y *et al.* (2020) Atg9 is a lipid scramblase that mediates autophagosomal membrane expansion. *Nat Struct Mol Biol* **27**, 1185–1193.
19 Melia TJ (2023) Growing thin – how bulk lipid transport drives expansion of the autophagosome membrane but not of its lumen. *Curr Opin Cell Biol* **83**, 102190.
20 Young LN and Villa E (2023) Bringing structure to cell biology with cryo-electron tomography. *Annu Rev Biophys* **52**, 573–595.
21 Bieber A, Capitanio C, Wilfling F, Plitzko J and Erdmann PS (2021) Sample preparation by 3D-correlative focused ion beam milling for high-resolution cryo-electron tomography. *J Vis Exp* **176**, doi: 10.3791/62886
22 Asano S, Engel BD and Baumeister W (2016) In situ cryo-electron tomography: a post-reductionist approach to structural biology. *J Mol Biol* **428** (2 Pt A), 332–343.
23 Plattner H and Bachmann L (1982) Cryofixation: a tool in biological ultrastructural research. *Int Rev Cytol* **79**, 237–304.
24 Dubochet J, McDowall AW, Menge B, Schmid EN and Lickfeld KG (1983) Electron microscopy of frozen-hydrated bacteria. *J Bacteriol* **155**, 381–390.
25 Huang Y, Zhang Y and Ni T (2023) Towards in situ high-resolution imaging of viruses and macromolecular complexes using cryo-electron tomography. *J Struct Biol* **215**, 108000.
26 Bieber A, Capitanio C, Erdmann PS, Fiedler F, Beck F, Lee CW, Li D, Hummer G, Schulman BA, Baumeister W *et al.* (2022) In situ structural analysis reveals membrane shape transitions during autophagosome formation. *Proc Natl Acad Sci USA* **119**, e2209823119.
27 Li M, Tripathi-Giesgen I, Schulman BA, Baumeister W and Wilfling F (2023) In situ snapshots along a mammalian selective autophagy pathway. *Proc Natl Acad Sci USA* **120**, e2221712120.
28 Carter SD, Mamede JI, Hope TJ and Jensen GJ (2020) Correlated cryogenic fluorescence microscopy and electron cryo-tomography shows that exogenous TRIM5alpha can form hexagonal lattices or autophagy aggregates in vivo. *Proc Natl Acad Sci USA* **117**, 29702–29711.
29 Osawa T and Noda NN (2019) Atg2: a novel phospholipid transfer protein that mediates de novo autophagosome biogenesis. *Protein Sci* **28**, 1005–1012.
30 Chowdhury S, Otomo C, Leitner A, Ohashi K, Aebersold R, Lander GC and Otomo T (2018) Insights into autophagosome biogenesis from structural and biochemical analyses of the ATG2A-WIPI4 complex. *Proc Natl Acad Sci USA* **115**, E9792–E9801.
31 Shpilka T, Welter E, Borovsky N, Amar N, Mari M, Reggiori F and Elazar Z (2015) Lipid droplets and their component triglycerides and steryl esters regulate autophagosome biogenesis. *EMBO J* **34**, 2117–2131.
32 Birmingham CL, Smith AC, Bakowski MA, Yoshimori T and Brumell JH (2006) Autophagy controls *Salmonella* infection in response to damage to the *Salmonella*-containing vacuole. *J Biol Chem* **281**, 11374–11383.
33 Horos R, Buscher M, Kleinendorst R, Alleaume AM, Tarafder AK, Schwarzl T, Dziuba D, Tischer C, Zielonka EM, Adak A *et al.* (2019) The small non-coding vault RNA1-1 acts as a Riboregulator of autophagy. *Cell* **176**, 1054–1067.e12.
34 Mandell MA, Jain A, Arko-Mensah J, Chauhan S, Kimura T, Dinkins C, Silvestri G, Münch J, Kirchhoff F, Simonsen A *et al.* (2014) TRIM proteins regulate autophagy and can target autophagic substrates by direct recognition. *Dev Cell* **30**, 394–409.
35 Li YL, Chandrasekaran V, Carter SD, Woodward CL, Christensen DE, Dryden KA, Pornillos O, Yeager M, Ganser-Pornillos BK, Jensen GJ *et al.* (2016) Primate TRIM5 proteins form hexagonal nets on HIV-1 capsids. *Elife* **5**, e16269.
36 Berger C, Dumoux M, Glen T, Yee NB, Mitchels JM, Patakova Z, Darrow MC, Naismith JH and Grange M

(2023) Plasma FIB milling for the determination of structures in situ. *Nat Commun* **14**, 629.
37 Gorelick S, Dierickx DA, Buckley G, Whisstock JC and De Marco A (2020) Assembly and imaging set up of PIE-scope. *Bio Protoc* **10**, e3768.
38 Klumpe S, Fung HK, Goetz SK, Zagoriy I, Hampoelz B, Zhang X, Erdmann PS, Baumbach J, Müller CW, Beck M *et al*. (2021) A modular platform for automated cryo-FIB workflows. *Elife* **10**, e70506.
39 Tacke S, Erdmann P, Wang Z, Klumpe S, Grange M, Plitzko J and Raunser S (2021) A streamlined workflow for automated cryo focused ion beam milling. *J Struct Biol* **213**, 107743.
40 Schaffer M, Pfeffer S, Mahamid J, Kleindiek S, Laugks T, Albert S, Engel BD, Rummel A, Smith AJ, Baumeister W *et al*. (2019) A cryo-FIB lift-out technique enables molecular-resolution cryo-ET within native *Caenorhabditis elegans* tissue. *Nat Methods* **16**, 757–762.
41 Biazik JM, Yla-Anttila P, Vihinen H, Jokitalo E and Eskelinen EL (2015) Ultrastructural relationship of the phagophore with surrounding organelles. *Autophagy* **11**, 439–451.
42 Wozny MR, Di Luca A, Morado DR, Picco A, Khaddaj R, Campomanes P, Ivanović L, Hoffmann PC, Miller EA, Vanni S *et al*. (2023) In situ architecture of the ER-mitochondria encounter structure. *Nature* **618**, 188–192.
43 Capitanio C, Bieber A and Wilfling F (2023) How membrane contact sites shape the phagophore. *Contact (Thousand Oaks)* **6**, 25152564231162495.
44 Weber MS, Wojtynek M and Medalia O (2019) Cellular and structural studies of eukaryotic cells by cryo-electron tomography. *Cell* **8**, 57.